Geophysical Research Letters

RESEARCH LETTER
10.1029/2022GL101697

Key Points:

- First high-resolution image of crustal structure in the core of the Eastern Himalayan Syntaxis is constructed from P receiver functions
- Two disconnected groups of low velocity zones are observed in upper to middle crust, which prevents the development of crust flow
- An intra-crustal interface and a Moho offset we find suggest that underthrusting and pure shear mechanisms dominate crustal deformation

Supporting Information:

Supporting Information may be found in the online version of this article.

Correspondence to:

Q. Xu and S. Pei,
xuqiang@itpcas.ac.cn;
peisp@itpcas.ac.cn

Citation:

Xu, Q., Ding, L., Pei, S., Yuan, X., Zhao, J., Liu, H., et al. (2022). Underthrusting and pure shear mechanisms dominate the crustal deformation beneath the core of the Eastern Himalayan Syntaxis as inferred from high-resolution receiver function imaging. *Geophysical Research Letters*, *49*, e2022GL101697. https://doi.org/10.1029/2022GL101697

Received 12 OCT 2022
Accepted 10 DEC 2022

Underthrusting and Pure Shear Mechanisms Dominate the Crustal Deformation Beneath the Core of the Eastern Himalayan Syntaxis as Inferred From High-Resolution Receiver Function Imaging

Qiang Xu[1], Lin Ding[1], Shunping Pei[1], Xiaohui Yuan[2], Junmeng Zhao[1], Hongbing Liu[1], Hanlin Liu[1], Lei Li[1], and Hong Zuo[1]

[1]State Key Laboratory of Tibetan Plateau Earth System, Environment and Resources (TPESER), Institute of Tibetan Plateau Research, Chinese Academy of Sciences, Beijing, China, [2]Deutsches GeoForschungsZentrum GFZ, Potsdam, Germany

Abstract How the crust in the core of the Eastern Himalayan Syntaxis (EHS) deforms responding to the India-Asia collision remains ambiguous. Here we present the first high-resolution receiver functions image of crustal structure along a new NW-SE trending dense nodal array crossing the core of the EHS. Two sets of low velocity zones (LVZs) are clearly observed: one with a flat style beneath the western Lhasa terrane and Higher Himalaya at 18–20 km depth and the other with two west-dipping shapes below the western Yarlung-Zangbo suture within 10–30 km depth. These LVZs caused by partial melting and aqueous fluids are disconnected, impeding the formation of crustal flow. A discontinuous east-dipping intra-crustal discontinuity and a sharp Moho offset of 7 km under the Aniqiao-Motuo shear zone are identified, suggesting that the underthrusting of the Indian lower crust and pure shear mechanisms jointly dominate crustal deformation in the core of the EHS.

Plain Language Summary The tectonic evolution of the Eastern Himalayan Syntaxis (EHS) involves complex tectonic activities such as collision, subduction, and rapid exhumation, making the EHS an ideal site for studying the dynamics of continental collision processes. Strong crustal shortening occurs during the formation of the EHS, but the specific mechanism that accommodates this crustal deformation remains unclear. In this study, we construct a novel seismic image of crustal structure with unprecedented details along a recently deployed dense nodal array that traverses the core of the EHS. We observe two unconnected groups of low velocity zones, which call into question the validity of the crustal flow model in the core of the EHS. Our observations indicate that the underthrusting of the Indian lower crust and pure shear mechanisms, rather than a model of vertically coherent deformation, account for the present crustal deformation in the core of the EHS.

1. Introduction

The Eastern Himalayan Syntaxis (EHS), also commonly called the Namcha Barwa Syntaxis, is situated at the eastern end of the Himalayan orogenic belt and is the product of the India-Asia collision initiated at 65–60 Ma and the subsequent continental convergence (e.g., Ding et al., 2017; Yin & Harrison, 2000). The inverse U-turn EHS is divided into three major tectonic-stratigraphic units (Figure 1): the Higher Himalaya (HH), the Yarlung-Zangbo suture (YZS), and the Lhasa terrane (LT) (W. C. Xu et al., 2013). The HH, the core of the EHS and also known as the Namcha Barwa metamorphic massif, is characterized by a NNE-oriented antiform and is bounded to the east by the right-lateral, strike-slip Aniqiao-Motuo shear zone (AMSZ) and to the west by the left-lateral, strike-slip Dongjiu-Milin shear zone (Figure 1) (Z. Q. Xu et al., 2012). Owing to its special geographical location, the EHS has experienced strong crustal shortening, which not only leads to the concentrated tectonic stress and frequent earthquakes, but also records the most wonderful tectonic scenarios involving collision, subduction-exhumation and high pressure metamorphism (e.g., Bracciali et al., 2016; Ding et al., 2001; Li et al., 2019). Therefore, it is crucial to elucidate the crustal deformation mechanism of the EHS for unraveling the tectonic evolution of the EHS and the dynamical processes of continental collision.

The vertical coherent deformation model, deduced from the joint analysis of the Global Positioning System (GPS) measurements, Quaternary fault slip rates, and shear wave splitting parameters, is suggested to describe the coupling deformation style between the crust and mantle around the core of the EHS (Chang et al., 2015). However, this model is invalid within the central EHS because the strain fields have been altered by the recent

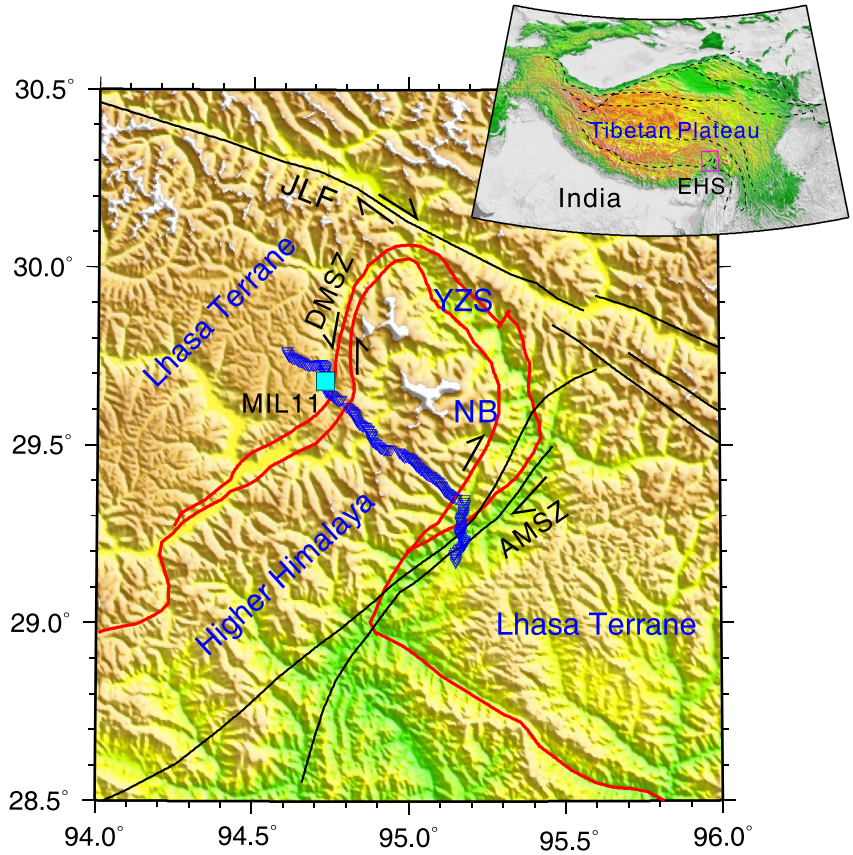

Figure 1. Topographic map of the Eastern Himalayan Syntaxis showing major tectonic divisions, faults, and the dense array of nodal seismometers used in this study (blue inverted triangles). Red lines indicate the Yarlung-Zangbo suture following Xu et al. (2012). The cyan square denotes the location of broadband seismic station MIL11 used for receiver function modeling. The purple rectangle on the inset map shows the location of the study region in a larger context. DMSZ, Dongjiu-Milin shear zone; AMSZ, Aniqiao-Motuo shear zone; NB, Namche Barwa peak; JLF, Jiali fault.

rapid exhumation of the Indian crust (Chang et al., 2015). In contrast, multiple geophysical data sets illustrate that the mid-lower crust of the EHS is characterized by low velocity (Hu & Yao, 2018; Hu et al., 2020), high attenuation (Zhao et al., 2013), and low resistivity (Dong et al., 2016; Lin et al., 2017). These features confirm the existence of crustal mechanically weak zones, which provide support for a clockwise mid-crustal channel flow around the core of the EHS (Beaumont et al., 2001; Huang et al., 2020). However, the depths and connectivity of these weak zones in the core of the EHS are unclear, partly due to the gap in station coverage caused by the harsh natural environment and the lack of road access. Accordingly, what mechanisms control the crustal deformation in the core of the EHS needs to be further clarified.

A comprehensive tectonic aneurysm model is present to focus on the interactions between the tectonic and surface processes (Koons et al., 2013; Zeitler et al., 2001). This model suggests that the efficient erosion weaken the upper crust, developing a feedback in which the deep materials that have experienced decompression melting form crust flow and then move rapidly to the surface (Zeitler et al., 2001). Meanwhile, the low velocity zone (LVZ) and the high conductivity layer near Namcha Barwa Peak satisfy the requirement of the tectonic aneurysm model (Hu & Yao, 2018; Lin et al., 2017). However, the results of valley bottom reconstruction and sediment dating propose that rapid rock uplift controls the high erosion rates within the Yarlung Tsangpo gorge (P. Wang et al., 2014), which is opposite to the tectonic aneurysm model. Thus, whether tectonics or surface processes trigger the feedback between them is still a very controversial topic.

Additionally, thermodynamic numerical predictions demonstrate that the 3-D geometry of a curved subduction slab is important for producing the observed deformation patterns and exhumation at syntaxes (Bendick & Ehlers, 2014). Tomographic images reveal that the subducting Indian plate reaches the Bangong-Nujiang suture

at depths of 100–150 km (Dubey et al., 2022), but the underthrusting of the Indian lower crust, which is widely reported in the Himalayan orogenic belt (Kumar et al., 2022), is rarely observed in the core of the EHS.

The recent rapid development of dense array observations provides an opportunity to delineate the detailed depth variations of crustal interfaces (Tian et al., 2021), which are advantageous to address the issues summarized above. Taking advantage of the first dense nodal seismic array that crosses the core of the EHS with a NW-SE trending (Figure 1), we aim to construct a high-resolution image of crustal structure using P receiver functions (PRFs). Our observations emphasize that the underthrusting and pure shear mechanisms jointly dominate the crustal deformation in the core of the EHS, which provide valuable new constraints on our understanding of the tectonic evolution of the EHS.

2. Data and Methods

We use seismic waveform data from a linear dense array of 200 SmartSolo IGU-16HR 3C seismometers (5 Hz) with a sampling frequency of 100 Hz. This array was deployed with an average station spacing of 500 m along the NW-SE trending Paimo road, which is under construction and provides access across the core of the EHS for the first time. These three-component nodal seismometers were operated for an average of 27 days in June 2021. The original waveforms of the selected 99 teleseismic earthquakes with magnitudes (Mb) greater than 5.0 and epicentral distance ranges of 30–95° (Figure S1 in Supporting Information S1) are windowed 20 s before and 100 s after the direct P wave arrival and band-pass filtered with corner frequencies of 0.05 and 5.0 Hz after removing the instrument response. We rotate the Z-N-E components of each event into the P-SV-SH components using the back azimuth and incidence angle, and then yield the SV receiver function (PRF) by deconvolving the SV component with the *P* component through a time-domain spiking deconvolution approach (Yuan et al., 1997). After visual inspection, we retain a total of 5,173 high quality PRFs for further analysis. Based on the distribution of the piercing points at a depth of 60 km (Figure 2a), we build a 2-D cross-section of summation traces by stacking the moveout corrected PRFs with piercing points spanning a 2 km distance along line AB in order to examine the overall quality of the PRFs. This strategy allows us to identify the clear Moho Ps conversions at 5–8 s (Figure 2b).

We generate a high-resolution depth migrated image using a common conversion point (CCP) stacking approach to enhance coherent features of crustal discontinuities (Dueker & Sheehan, 1997). We divide the subsurface volume into grids with sizes of 1.0 km in the horizontal distance and 0.5 km in depth along line AB, and then back-project the amplitudes of each PRF along their incident ray paths to the actual locations where the Ps conversions occur. Finally, we average the amplitudes within the range of a Fresnel zone to produce a smooth 2-D structural image. The ray tracing is performed using the region crustal velocity model from the direct inversion of phase velocity dispersion curves (Huang et al., 2020).

3. Results

The CCP image exhibits significant lateral variations of crustal interfaces beneath the core of the EHS (Figure 3a). The most prominent feature is a strong positive conversion (red color) at depths of 47–60 km, which is interpreted as the Moho. The Moho shallows gently from 60 km in the LT at the western end of the profile to 54 km below the central HH, before deepening to 57 km near the AMSZ. Farther east, the Moho abruptly shallows to 50 km below the AMSZ with a sharp offset of 7 km, and further shallows gradually to 47 km in the LT at the eastern end of the profile. Above the Moho, an east-dipping discontinuous positive phase (C) in the depth range of 35–50 km is well resolved and may be indicative of an intra-crustal interface that covers the LT and most of the HH in the western portion of the profile. In addition, two sets of discrete negative conversions (blue color) are observed: one with a flat signal (N1) at depths of 18–20 km below the LT in the west and the HH and the other with two west-dipping phases (N2 and N3) within 15–30 km depth under the western YZS. These negative phases represent the tops of LVZs within the upper to middle crust.

We also evaluate the stability of the CCP image by a bootstrap resampling technique (Efron & Tibshirani, 1986). We conduct 100 CCP stacks with different data sets formed by randomly selecting the same number of PRFs from the original PRFs, and then calculate the standard deviation of each grid using these 100 stacking values. We consider the grids with amplitudes larger than 2.0 standard deviations where our interpreted discontinuities are located as very convincing observations (Figure 3b).

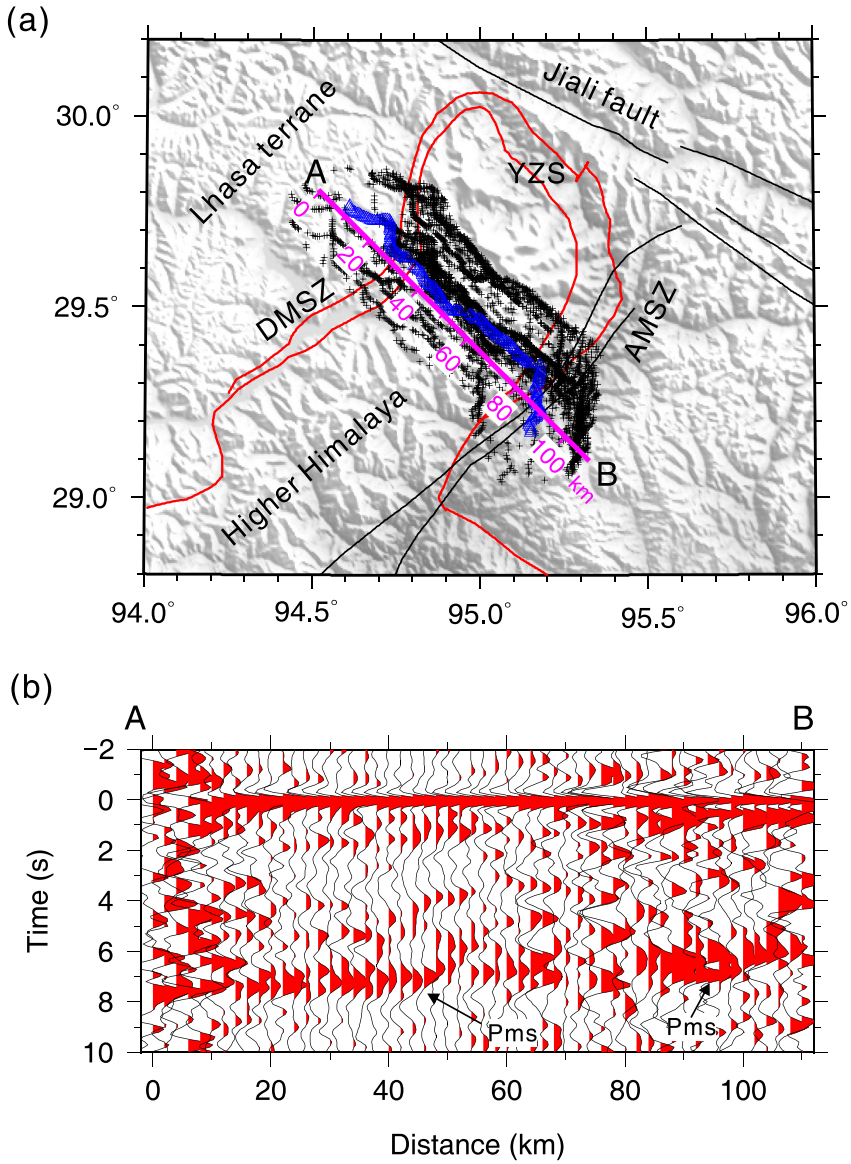

Figure 2. (a) Piercing points (black crosses) of all P receiver functions (PRFs) at a depth of 60 km. The magenta line AB showing distance values marks the location of the section in Figure 3. (b) Stacked traces of PRFs after moveout correction within a 2 km bin along line AB based on the locations of piercing points. Two black arrows illustrate the Ps conversions from Moho (Pms).

The depth uncertainties at our interpreted interfaces originate mainly from the reference velocity model chosen during the CCP stacking. We perform tests of the CCP stacking using another two crustal models with Vp = 6.3 km/s and Vp/Vs ratios of 1.7 and 1.8, respectively. By comparing the Moho depths determined from the CCP stacking images using the two test models mentioned above and our preferred model, we find that the maximum deviation of Moho depths is less than 5 km, which has a negligible impact on our interpretations (Figure S2 in Supporting Information S1).

4. Discussion

In the following, we explore possible implications of the LVZs, an intra-crustal interface, and a Moho offset, in combination with existing geological and geophysical studies. Figure 4 summarizes our reasonable explanations of the key features of the CCP image.

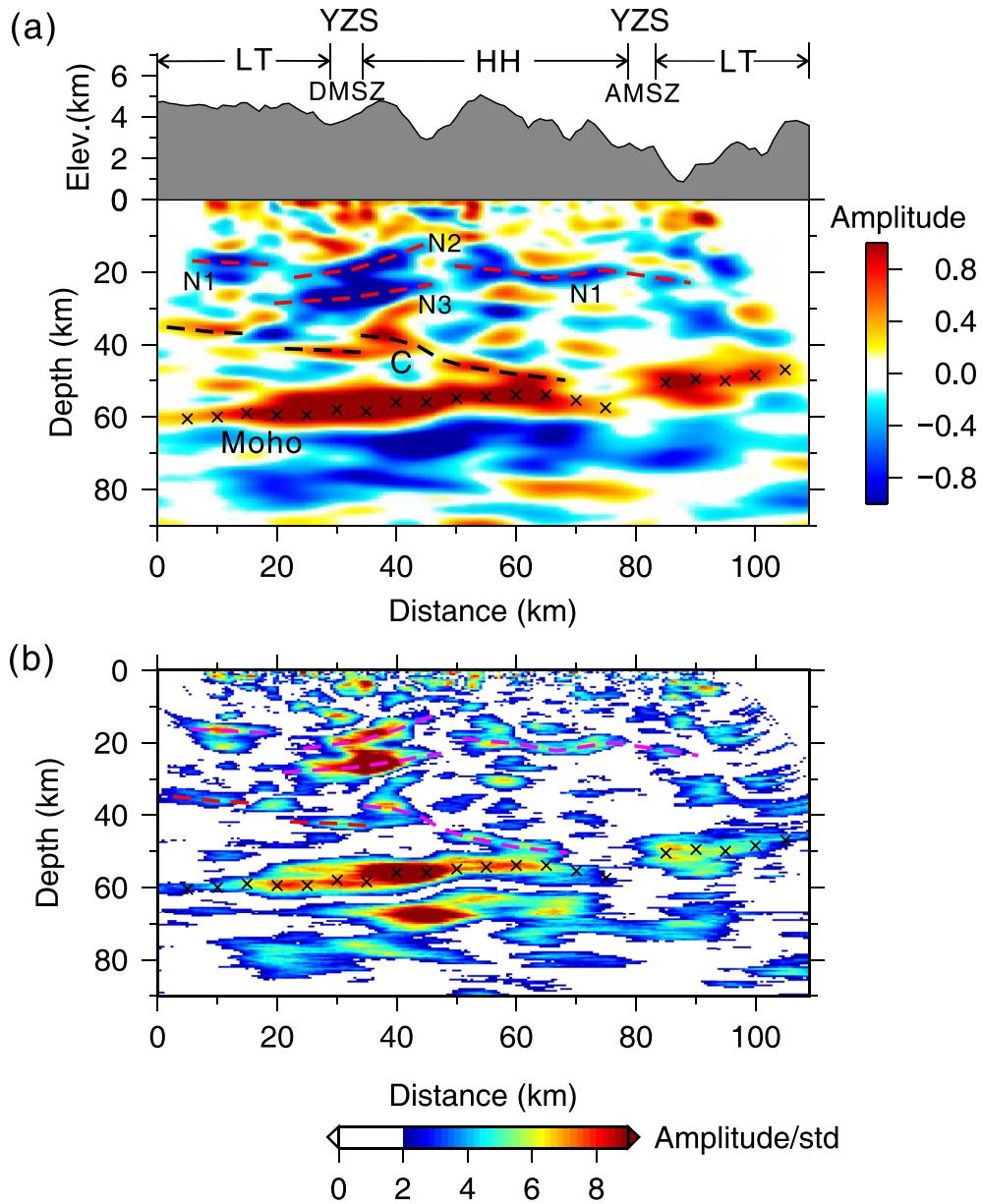

Figure 3. (a) PRFs common conversion point (CCP) stacking image of crustal structure along line AB (shown in Figure 2a). Topography with positions of major tectonic provinces and faults are presented in the top panel. Low velocity zones with negative amplitudes are marked by red dashed lines and denoted by N1, N2, and N3. The prominent intra-crustal interface labeled by C and Moho with positive amplitudes are marked by black dashed lines and black crosses, respectively. (b) Amplitude deviation defined by the ratio of amplitude to standard deviation for each grid in the CCP stacking section, superimposed by our interpretation of Moho and intra-crustal interfaces. LT, Lhasa terrane; HH, Higher Himalaya.

4.1. Insights Into the LVZs Within the Crust

The intra-crustal LVZ plays a vital role in the tectonic evolution of the Tibetan Plateau (e.g., Nelson et al., 1996). The crustal velocity structure determined in the earlier studies has a lower spatial resolution since the station spacing is typically >10 km (Hu & Yao, 2018; Huang et al., 2020), while our high-resolution crustal image illustrates two groups of pronounced LVZs with a 1 km spatial resolution (Figures 3 and 4). One group is the nearly flat LVZ N1 between 18 and 20 km depth over most of the section, and this corresponds well with the low velocity and high conductivity layer in the middle and upper crust of central Tibet on both sides of the YZS. The other group consists of two west-dipping LVZs at depths of 10–30 km beneath the western YZS, and these

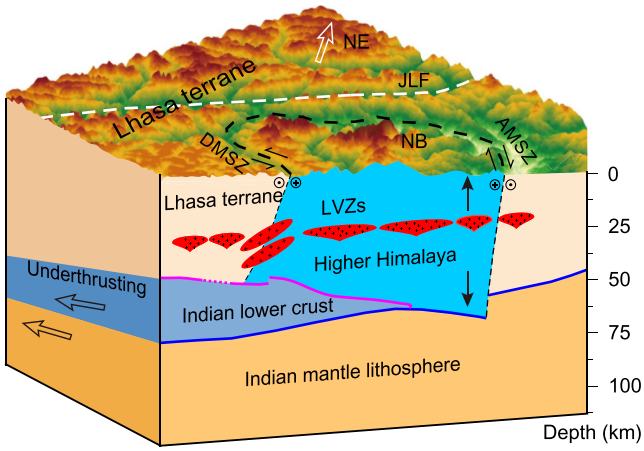

Figure 4. Diagram showing the present crustal deformation beneath the core of the Eastern Himalayan Syntaxis characterized by the underthrusting of the Indian lower crust and pure shear mechanisms.

are not only consistent with the location of the high conductivity layer in this localized region, but also probably connect westward with the mid-crustal LVZ in the western EHS (Hu et al., 2020; Lin et al., 2017). Furthermore, we obtain a shear wave velocity model for broadband station MIL11 near the western YZS by the PRF forward modeling. This model clearly reveals the existence of two LVZs with a minimum of 3.2 km/s at depths of 12.5 and 25 km, respectively, which verifies the reliability of our observations (Figure S3 in Supporting Information S1).

Following previous findings, we interpret these observed LVZs as the likely joint effects of partial melting and aqueous fluids (e.g., Nelson et al., 1996; Xie et al., 2021; Q. Xu et al., 2015). We speculate that the water could have been released either from the basal erosion of the overlying Tibetan crust or from dehydration reaction in the metamorphic rocks. The presence of water can significantly reduce melting temperature, thus contributing to the generation of partial melting. The mechanisms that could account for the crustal partial melting include rapid decompression and the absorption of heat from radiogenic heating, strain heating, and asthenospheric upwelling along tearing windows (Xie et al., 2021), but other possible mechanisms cannot be ruled out. The LVZs N1 and N2 may be associated with the higher-grade metamorphic rocks exposed near Namcha Barwa peak (NB), providing support for the tectonic aneurysm model in extreme localized area. In addition, these two groups of LVZs with different geometries are disconnected, and this feature together with the low to moderate crustal Vp/Vs ratios of 1.696–1.742 (Peng et al., 2017; C. Y. Wang et al., 2019), bring into question the development of crust flow in the core of the EHS.

4.2. Implications of the Moho Offset and Intra-Crustal Interface

The Moho is the most striking discontinuity in the CCP image. We generate a Moho depth map of the EHS using the earlier observations (Peng et al., 2017; C. Y Wang et al., 2019; Q Xu et al., 2013) and our estimates in this study (Figure S4 in Supporting Information S1). The Moho depth generally varies from 47 to 75 km, while the Moho beneath the HH is shallower than 60 km and grows deeper toward the western and northern LT, forming a convex structure under the core of the EHS. Previous thermokinematic studies suggest that the denudation rate at the Namche Barwa massif is 7–9 mm/yr (Enkelmann et al., 2011); if this status persists for 10 Ma, the entire crust will be removed by surface denudation, which is unlikely to happen. Accordingly, we suggest that the Moho uplift, rather than the surface denudation, probably drives the rapid uplift of the core of the EHS since 7–6 Ma.

Furthermore, the sharp Moho offset of 7 km under the AMSZ is found by our observations for the first time to the best of our knowledge (Figures 3 and 4). For the bins during CCP stacking where the Moho offset is located, the number of stacked PRFs is greater than 50 (Figure S5 in Supporting Information S1), which guarantees that this Moho offset is not an artifact of the imaging. This Moho offset may be regarded as the boundary between the HH and the LT in the east. We propose that the formation of the Moho offset is probably the manifestation of pure shear deformation of the HH (Figure 4). The calculated kinematic vorticity numbers at stations located near our profile are 0.3, which imply that the lithospheric deformation style is inclined to pure shear (Chang et al., 2015). This inference further strengthens our interpretation. Compared with the surrounding LT, the HH exhibits a higher shear wave velocity (>3.4 km/s) in the depth range of 35–50 km determined using ambient noise dispersion data (Hu et al., 2020), indicating the rigidity of the lower crust in the core of the EHS. Under a principal compressive stress that is oriented NNE-SSW, the rigid lower crust of the eastern HH has been undergoing vertical growth, which easily leads to the formation of the Moho offset during crustal thickening. Another alternative model for the cause of the Moho offset is eastward subduction. Given the absence of overlapping Moho interfaces and the presence of dextral strike slip faults, there is no convincing evidence for this model of eastward subduction.

Previous studies have proved that the underthrusting Indian lower crust reaches varying latitudes below the southern LT, and undergoes partial eclogitization or underplating by mantle mafic materials (Kumar et al., 2022; Shi et al., 2016; Q. Xu et al., 2017). Three NE-trending PRFs sections crossing the EHS and surrounding area have revealed that the underthrusting Indian lower crust extends beyond at least the Jiali fault (C. Y. Wang et al., 2019). Accordingly, we interpret the observed discontinuous intra-crustal interface C to represent the top

boundary of the underthrusting Indian lower crust (Figures 3 and 4). A supporting evidence for this interpretation is that the *P-T* conditions of high-pressure granulite from the EHS also indicate that the Indian continental crust underthrusted to at least 50–55 km depth (Zhang et al., 2022). Confined by the east-dipping feature of this top interface, the Indian lower crust thins dramatically toward the east and finally disappears at the eastern edge of the HH. A plausible mechanism for this phenomenon is the delamination or foundering of mafic lower crust during the uneven thickening of the crust in HH. This process may be triggered by the negative buoyancy due to the eclogitization of Indian lower crust and also explain why the crust is compose of a felsic to intermediate bulk composition in our study area reported by the previous receiver function studies (Peng et al., 2017; C Y Wang et al., 2019).

5. Conclusions

We present a high-resolution migrated image of crustal structure through the core of the EHS using PRFs based on teleseismic waveforms recorded by a dense NW-SE nodal array. Two sets of LVZs are clearly imaged: one with a sub-horizontal shape beneath the western LT and HH at depths of 18–20 km and the other with west-dipping morphologies below the western YZS in the depth range of 15–30 km. These LVZs originate as a result of crustal partial melting and aqueous fluids, but their lack of connectivity hinders the formation of crustal flow. More importantly our image displays a discontinuous intra-crustal interface beneath the western LT and most of the HH as well as a prominent Moho offset of 7 km under the AMSZ, which suggest that the underthrusting of the Indian lower crust and pure shear are the predominant mechanisms of crustal deformation in the core of the EHS, in contrast with the model of vertical coherent deformation around the core of the EHS. These new observations provide unprecedented structural details that will shed light on the tectonic evolution of the EHS and continental collision processes.

Data Availability Statement

The receiver functions waveforms used in this study are publicly available at https://doi.org/10.5281/zenodo.7135118. Most of our figures are produced with the Generic Mapping Tools (Wessel & Smith, 1998).

Acknowledgments
We thank Yunxiang Yang and Qingxian Lu from China Huaneng for their assistance in the field work. Constructive comments from two anonymous reviewers help us improve the original manuscript. This work is jointly funded by the National Natural Science Foundation of China (42074113), the Second Tibetan Plateau Scientific Expedition and Research Program (2019QZKK0708) and the K.C. Wong Education Foundation (GJTD-2019-04).

References

Beaumont, C., Jamieson, R. A., Nguyen, M. H., & Lee, B. (2001). Himalayan tectonics explained by extrusion of a low-viscosity crustal channel coupled to focused surface denudation. *Nature*, *414*(6865), 738–742. https://doi.org/10.1038/414738a

Bendick, R., & Ehlers, T. A. (2014). Extreme localized exhumation at syntaxes initiated by subduction geometry. *Geophysical Research Letters*, *41*(16), 5861–5867. https://doi.org/10.1002/2014gl061026

Bracciali, L., Parrish, R. R., Najman, Y., Smye, A., Carter, A., & Wijbrans, J. R. (2016). Pliod. *Earth-Science Reviews*, *160*, 350–385. https://doi.org/10.1016/j.earscirev.2016.07.010

Chang, L. J., Flesch, L. M., Wang, C. Y., & Ding, Z. F. (2015). Vertical coherence of deformation in lithosphere in the eastern Himalayan syntaxis using GPS, Quaternary fault slip rates, and shear wave splitting data. *Geophysical Research Letters*, *42*(14), 5813–5819. https://doi.org/10.1002/2015gl064568

Ding, L., Maksatbek, S., Cai, F. L., Wang, H. Q., Song, P. P., Ji, W. Q., et al. (2017). Processes of initial collision and suturing between India and Asia. *Science China Earth Sciences*, *60*(4), 635–651. https://doi.org/10.1007/s11430-016-5244-x

Ding, L., Zhong, D. L., Yin, A., Kapp, P., & Harrison, T. M. (2001). Cenozoic structural and metamorphic evolution of the eastern Himalayan syntaxis (Namche Barwa). *Earth and Planetary Science Letters*, *192*(3), 423–438. https://doi.org/10.1016/S0012-821x(01)00463-0

Dong, H., Wei, W. B., Jin, S., Ye, G. F., Zhang, L. T., Jing, J. E., et al. (2016). Extensional extrusion: Insights into South-eastward expansion of Tibetan Plateau from magnetotelluric array data. *Earth and Planetary Science Letters*, *454*, 78–85. https://doi.org/10.1016/j.epsl.2016.07.043

Dubey, A. K., Singh, A., Kumar, M. R., Jana, N., Sarkar, S., Saikia, D., & Singh, C. (2022). Tomographic imaging of the plate geometry beneath the Arunachal Himalaya and Burmese subduction zones. *Geophysical Research Letters*, *49*(8), e2022GL098331. https://doi.org/10.1029/2022GL098331

Dueker, K. G., & Sheehan, A. F. (1997). Mantle discontinuity structure from midpoint stacks of converted P–S waves across the Yellowstone hotspot track. *Journal of Geophysical Research*, *102*(B4), 8313–8327. https://doi.org/10.1029/96jb03857

Efron, B., & Tibshirani, R. (1986). Bootstrap methods for standard errors, confidence intervals, and other measures of statistical accuracy. *Statistical Science*, *1*, 54–75. https://doi.org/10.1214/ss/1177013815

Enkelmann, E., Ehlers, T. A., Zeitler, P. K., & Hallet, B. (2011). Denudation of the Namche Barwa antiform, eastern Himalaya. *Earth and Planetary Science Letters*, *307*(3–4), 323–333. https://doi.org/10.1016/j.epsl.2011.05.004

Hu, S. Q., & Yao, H. J. (2018). Crustal velocity structure around the eastern Himalayan Syntaxis: Implications for the nucleation mechanism of the 2017 M-s 6.9 Mainling earthquake and regional tectonics. *Tectonophysics*, *744*, 1–9. https://doi.org/10.1016/j.tecto.2018.06.006

Hu, S. Q., Yao, H. J., & Huang, H. (2020). Direct surface wave radial anisotropy tomography the crust of the eastern himalayan syntaxis. *Journal of Geophysical Research-Solid Earth*, *125*(5), e2019JB018257. https://doi.org/10.1029/2019JB018257

Huang, S. Y., Yao, H. J., Lu, Z. W., Tian, X. B., Zheng, Y., Wang, R., et al. (2020). High-resolution 3-D shear wave velocity model of the Tibetan plateau: Implications for crustal deformation and porphyry Cu deposit formation. *Journal of Geophysical Research-Solid Earth*, *125*(7), e2019JB019215. https://doi.org/10.1029/2019JB019215

Koons, P. O., Zeitler, P. K., & Hallet, B. (2013). Tectonic aneursms and mountain building. *Treatise on Geomorphology*, *5*, 318–349. https://doi.org/10.1016/B978-0-12-374739-6.00094-4

Kumar, V., Rai, S. S., Hawkins, R., & Bodin, T. (2022). Seismic imaging of crust beneath the western Tibet-Pamir and western Himalaya using ambient noise and earthquake data. *Journal of Geophysical Research-Solid Earth*, *127*(6), e2021JB022574. https://doi.org/10.1029/2021JB022574

Li, W., Xu, C. J., Yi, L., Wen, Y. M., & Zhang, X. (2019). Source parameters and seismogenic structure of the 2017 Mw 6.5 mainling earthquake in the eastern Himalayan syntaxis (Tibet, China). *Journal of Asian Earth Sciences*, *169*, 130–138. https://doi.org/10.1016/j.jseaes.2018.07.027

Lin, C. H., Peng, M., Tan, H. D., Xu, Z. Q., Li, Z. H., Kong, W. X., et al. (2017). Crustal structure beneath Namche Barwa, eastern Himalayan syntaxis: New insights from three-dimensional magnetotelluric imaging. *Journal of Geophysical Research-Solid Earth*, *122*(7), 5082–5100. https://doi.org/10.1002/2016jb013825

Nelson, K. D., Zhao, W. J., Brown, L. D., Kuo, J., Che, J. K., Liu, X. W., et al. (1996). Partially molten middle crust beneath southern Tibet: Synthesis of project INDEPTH results. *Science*, *274*(5293), 1684–1688. https://doi.org/10.1126/science.274.5293.1684

Peng, M., Jiang, M., Chen, Y. L., Tan, H. D., Li, Q. Q., Zhang, L. S., & Xu, L. H. (2017). Crustal structure under the eastern Himalayan syntaxis seismic array and its geodynamic implications derived from receiver functions. *Chinese Journal of Geophysics-Chinese Edition*, *60*(1), 70–85. https://doi.org/10.6038/cjg20170107

Shi, D. N., Zhao, W. J., Klemperer, S. L., Wu, Z. H., Mechie, J., Shi, J. Y., et al. (2016). West-East transition from underplating to steep subduction in the India-Tibet collision zone revealed by receiver-function profiles. *Earth and Planetary Science Letters*, *452*, 171–177. https://doi.org/10.1016/j.epsl.2016.07.051

Tian, X. B., Bai, Z. M., Klemperer, S. L., Liang, X. F., Liu, Z., Wang, X., et al. (2021). Crustal-scale wedge tectonics at the narrow boundary between the Tibetan Plateau and Ordos block. *Earth and Planetary Science Letters*, *554*, 116700. https://doi.org/10.1016/j.epsl.2020.116700

Wang, C. Y., Mooney, W. D., Zhu, L., Wang, X., Lou, H., You, H., et al. (2019). Deep structure of the eastern Himalayan collision zone: Evidence for underthrusting and delamination in the postcollisional stage. *Tectonics*, *38*(10), 3614–3628. https://doi.org/10.1029/2019tc005483

Wang, P., Scherler, D., Jing, L. Z., Mey, J., Avouac, J. P., Zhang, Y. D., & Shi, D. G. (2014). Tectonic control of Yarlung Tsangpo gorge revealed by a buried canyon in southern Tibet. *Science*, *346*(6212), 978–981. https://doi.org/10.1126/science.1259041

Wessel, P., & Smith, W. H. F. (1998). New, improved version of generic mapping tools released. *EOS, Transactions American Geophysical Union*, *79*(47), 579. https://doi.org/10.1029/98EO00426

Xie, C. L., Jin, S., Wei, W. B., Ye, G. F., Jing, J. N., Zhang, L. T., et al. (2021). Middle crustal partial melting triggered since the mid-miocene in southern Tibet: Insights from magnetotelluric data. *Journal of Geophysical Research-Solid Earth*, *126*(9), e2021JB022435. https://doi.org/10.1029/2021JB022435

Xu, Q., Zhao, J. M., Pei, S. P., & Liu, H. B. (2013a). Imaging lithospheric structure of the eastern Himalayan syntaxis: New insights from receiver function analysis. *Journal of Geophysical Research-Solid Earth*, *118*(5), 2323–2332. https://doi.org/10.1002/jgrb.50162

Xu, Q., Zhao, J. M., Yuan, X. H., Liu, H. B., & Pei, S. P. (2015). Mapping crustal structure beneath southern Tibet: Seismic evidence for continental crustal underthrusting. *Gondwana Research*, *27*(4), 1487–1493. https://doi.org/10.1016/j.gr.2014.01.006

Xu, Q., Zhao, J. M., Yuan, X. H., Liu, H. B., & Pei, S. P. (2017). Detailed configuration of the underthrusting Indian lithosphere beneath Western Tibet revealed by receiver function images. *Journal of Geophysical Research-Solid Earth*, *122*(10), 8257–8269. https://doi.org/10.1002/2017jb014490

Xu, W. C., Zhang, H. F., Harris, N., Guo, L., & Pan, F. B. (2013b). Rapid Eocene erosion, sedimentation and burial in the eastern Himalayan syntaxis and its geodynamic significance. *Gondwana Research*, *23*(2), 715–725. https://doi.org/10.1016/j.gr.2012.05.011

Xu, Z. Q., Ji, S. C., Cai, Z. H., Zeng, L. S., Geng, Q. R., & Cao, H. (2012). Kinematics and dynamics of the Namche Barwa syntaxis, eastern Himalaya: Constraints from deformation, fabrics and geochronology. *Gondwana Research*, *21*(1), 19–36. https://doi.org/10.1016/j.gr.2011.06.010

Yin, A., & Harrison, T. M. (2000). Geologic evolution of the Himalayan-Tibetan orogen. *Annual Review of Earth and Planetary Sciences*, *28*(1), 211–280. https://doi.org/10.1146/annurev.earth.28.1.211

Yuan, X. H., Ni, J., Kind, R., Mechie, J., & Sandvol, E. (1997). Lithospheric and upper mantle structure of southern Tibet from a seismological passive source experiment. *Journal of Geophysical Research*, *102*(B12), 27491–27500. https://doi.org/10.1029/97jb02379

Zeitler, P. K., Meltzer, A. S., Koons, P. O., Craw, D., Hallet, B., Chamberlain, C. P., et al. (2001). Erosion, Himalayan geodynamics, and the geomorphology of metamorphism. *Geological Society of America Today*, *11*(1), 4–9. https://doi.org/10.1130/1052-5173(2001)011<0004:ehgatg>2.0.co;2

Zhang, Z., Ding, H., Palin, R. M., Dong, X., Tian, Z., Kang, D., et al. (2022). On the origin of high-pressure mafic granulite in the Eastern Himalayan Syntaxis: Implications for the tectonic evolution of the Himalayan orogen. *Gondwana Research*, *104*, 4–22. https://doi.org/10.1016/j.gr.2021.05.011

Zhao, L. F., Xie, X. B., He, J. K., Tian, X. B., & Yao, Z. X. (2013). Crustal flow pattern beneath the Tibetan Plateau constrained by regional Lg-wave Q tomography. *Earth and Planetary Science Letters*, *383*, 113–122. https://doi.org/10.1016/j.epsl.2013.09.038